Journal of Solid State Chemistry **156,** 44–50 (2001)
doi:10.1006/jssc.2000.8956, available online at http://www.idealibrary.com on IDEAL®

Structure and Physical Properties of $BaCu_2Te_2$

Ying C. Wang and Francis J. DiSalvo

Department of Chemistry and Chemical Biology, Baker Laboratory, Cornell University, Ithaca, New York 14853

Received June 6, 2000; in revised form August 8, 2000; accepted September 5, 2000; published online December 21, 2000

$BaCu_2Te_2$ was synthesized at 690°C and its structure was determined via the Rietveld refinement method using powder X-ray diffraction with $R_p/wR_p(\%) = 4.01/5.36$. $BaCu_2Te_2$ crystallizes in the orthorhombic space group *Pnma* (No. 62) with $Z = 4$ and $a = 10.1244(5)$ Å, $b = 4.4577(3)$ Å, $c = 11.4642(6)$ Å, $V = 517.85(5)$ Å^3. It adopts the same structure type as α-$BaCu_2S_2$/$BaCu_2Se_2$/$BaZn_2Sb_2$. In $BaCu_2Te_2$, distorted $CuTe_4$ tetrahedra connect with one another by edge-sharing and corner-sharing to build up a three-dimensional framework. There is no structural resemblance between $BaCu_2Te_2$ and Cu_2Te (*P6/mmm*), but remarkably, the $BaCu_2Te_2$ framework is topologically identical to the net found in the mineral feldspar. Electrical property measurements on a sintered pellet indicate that it is a *p*-type degenerate semiconductor. An anomaly was observed in the variation of electrical resistivity as a function of temperature near 65 K. © 2001 Academic Press

INTRODUCTION

Copper-containing chalcogenides have displayed interesting properties such as mixed-valence, high electrical conductivity, and often Cu ion conductivity (1–5). Some representatives of these compounds exhibit very intriguing structural characteristics. Copper chalcogenide films are also used in several electronic and optical devices (6).

Among the plethora of copper-containing compounds, Cu_2Te, a semiconductor with a defect structure, deserves special attention (6–10). Cu_2Te has stimulated wide investigation in the category of so-called self-doping compounds (8–10). Stoichiometric Cu_2Te does not exist in nature; only minerals with composition close to $Cu_{1.7}Te$ have been found. It always shows a *p*-type conductivity behavior, independent of preparation methods (9,10). $Cu_{2-x}Te$ has a range of homogeneity between $Cu_{1.67}Te$ and Cu_2Te. According to the doping level, Cu_2Te can be classified into three types (9,10): (1) nondegenerate semiconductor with $x < 0.025$, which must be grown by special methods; (2) degenerate semiconductor with $0.03 < x < 0.10$; and (3) strongly degenerate semiconductor with $x > 0.1$, which can be synthesized by any method without difficulty. $Cu_{2-x}Te$ has both direct and indirect band gaps (8–10). The direct energy gap E_{gd} increases as x increases, but the indirect gap E_{gi} decreases as x increases. For $x = 0$, $E_{gd} = 1.18$ eV, $E_{gi} = 0.82$ eV. In the liquid state, Cu_2Te is an intrinsic semiconductor with $E_g = 0.65$ eV (9).

Further, $Cu_{2-x}Te$ has been considered as a promising thermoelectric material because of its high Seebeck coefficient in the moderate- to high-temperature range (9, 12–14).

Thus, it would be worthwhile to investigate ternary copper tellurides. A number of ternary copper tellurides have been synthesized (2,3,15), for example, Cu_2MTe_3 (M = Ti, Zr, Hf), $Cu_{1.85}Zr_2Te_6$, $A_3Cu_8Te_{10}$ (A = Rb, Cs), $K_4Cu_8Te_{11}$, $K_2Cu_5Te_5$, and $TlCu_3Te_2$. Two mixed alkali metal and alkaline earth metal quaternary compounds have been reported: $NaBa_6Cu_3Te_{14}$ and $(K_{0.6}Ba_{0.4})Ba_6Cu_{2.58}Te_{14}$ (2d). However, among the ternary copper-containing chalcogenides, there has been no report of alkaline earth metal copper tellurides. Further, although $BaCu_2S_2$ (16,17) and $BaCu_2Se_2$ (17) have been synthesized, their telluride analogue has not been reported. This paper presents our study of the structure and properties of $BaCu_2Te_2$, a new ternary barium copper telluride.

EXPERIMENTAL SECTION

All manipulations were carried out in an argon-filled glove box. The starting materials were (1) barium, distilled dendritic pieces (Aldrich), 99.9 + % purity, ampouled under argon; (2) copper (Cerac), 99.999% purity, − 100 mesh; (3) tellurium lumps (Johnson Matthey), 99.9999% purity. Stoichiometric elements were mixed in a vitreous carbon crucible (EMC) sealed in a silica tube and heated at 700°C or higher temperature for one week. Powder X-ray diffraction (Scintag XDA 2000, Cu$K\alpha$, 25°C) and microprobe analysis (JEOL 733 superprobe) revealed a ternary unknown phase and the known binary phases of BaTe and $Cu_{2-x}Te$. The sample was ground and pressed into a pellet under an Ar atmosphere. It was annealed in a sealed silica tube at 690°C for 3 weeks. Microprobe analysis indicated a homogeneous ternary phase. On the powder X-ray diffraction pattern, the diffraction lines from BaTe and $Cu_{2-x}Te$

0022-4596/01 $35.00

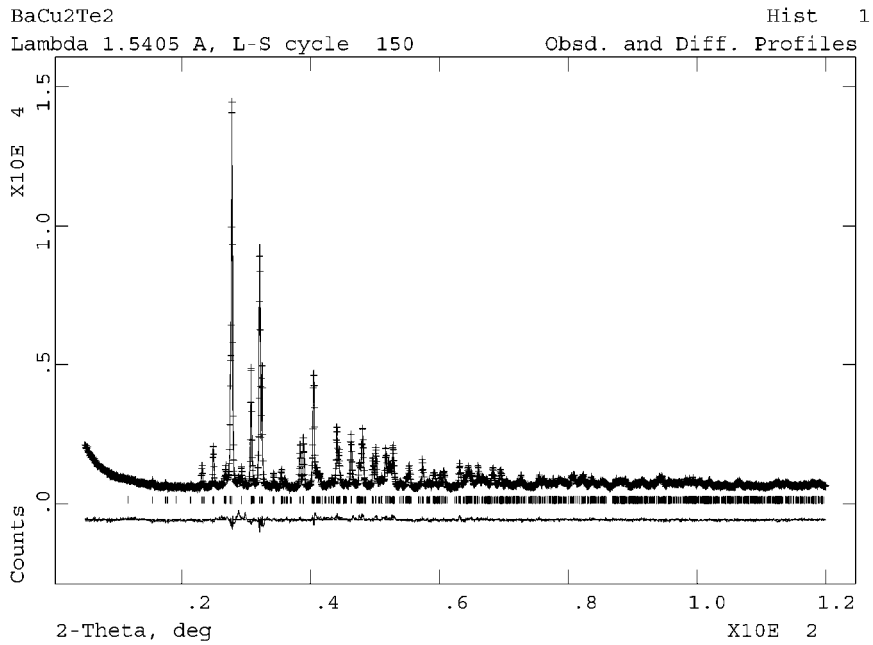

FIG. 1. Observed (+), calculated, and difference (bottom) X-ray powder diffraction pattern of $BaCu_2Te_2$ by using GSAS (18).

disappeared; all the lines could be indexed to an orthorhombic cell and the pattern is similar to that of $BaCu_2Se_2$. Based on the isostructural model of $BaCu_2Se_2$ (*Pnma*), the structure of $BaCu_2Te_2$ was refined by the Rietveld method using GSAS (18). The plot of final profile refinement is shown in Fig. 1. The relevant refinement information is listed in Table 1. Structural data are listed in Tables 2 and 3. The new phase was stable in air and no compositional change was observed after exposure in air for one year.

To measure transport properties, the pellet was cut into a rectangular bar ($4.2 \times 6.1 \times 6.2\ mm^3$) using a diamond-impregnated string saw (South Bay Tech.) and polished further by filing. Electrical resistivities were measured by using standard 4-probe AC techniques. Current contacts to the ends of the sample bar were made with ultrasonic indium and 0.05-mm-thick copper foil strips. Voltage leads were made by placing 38 AWG copper wires coated with silver epoxy (H20E, Epoxy Technology) onto a flat face of the sample. The thermopower and thermal conductivity were measured on the sample by using homebuilt thermopower and thermal conductivity measurement apparatus described elsewhere (19). The sample was initially mounted on a copper base with an indium solder. A 5-kΩ resistor was attached to the opposite end of the sample by an indium solder. Two 40 AWG Au,Fe (0.07%):Chromel-*p* thermocouples were placed in the indium joints at both ends of the

TABLE 1
Summary of Refinement Data and Lattice Parameters of $BaCu_2Te_2$

Formula	$BaCu_2Te_2$
Space group	*Pnma*
a (Å)	10.1244(5)
b (Å)	4.4577(3)
c (Å)	11.4742(6)
V (Å^3)	517.85(5)
Z	4
Calculated density	6.665 g/cm^3
Detector	HP Ge low-energy photon spectrometer
Counting time	5.5 s
Step	0.015°
Profile function	Pseudo-Voigt
Number of profile points	7666
Number of parameters refined	42
R_p (%)	4.01
wR_p (%)	5.36
R_B (%)	8.10
GOF	1.60
Durbin–Watson statistics	0.779

TABLE 2
Atomic Parameters and Standard Deviation for $BaCu_2Te_2$

	Wyckoff	*x*	*y*	*z*	$100U_{iso}$ (Å^2)	Occ
Ba	4c	0.2600(2)	0.75	0.3223(2)	2.22(7)	1
Cu1	4c	0.0558(4)	0.25	0.1098(4)	2.6(1)	1
Cu2	4c	0.4265(4)	0.75	0.0418(4)	2.9(1)	1
Te1	4c	0.4797(2)	0.25	0.1710(2)	1.26(6)	1
Te2	4c	0.1610(2)	0.75	0.0396(3)	1.63(6)	1

TABLE 3
Selected Bond Distances and Angles for $BaCu_2Te_2$

Distances (Å)			
2 × Ba–Te1	3.596(2)	2 × Cu2–Cu2	2.847(5)
2 × Ba–Te1	3.609(2)		
2 × Ba–Te2	3.438(2)		
Ba–Te2	3.396(3)		
Cu1–Te1	2.630(5)	2 × Cu2–Te1	2.731(3)
2 × Cu1–Te2	2.599(2)	Cu2–Te1	2.620(4)
Cu1–Te2	2.784(5)	Cu2–Te2	2.688(5)
Angles (°)			
Te1–Cu1–Te2	111.0(2)	Te1–Cu2–Te1	109.4(2)
2 × Te1–Cu1–Te2	114.6(1)	2 × Te1–Cu2–Te1	115.8(1)
2 × Te2–Cu1–Te2	97.6(1)	2 × Te1–Cu2–Te2	101.7(1)
Te2–Cu1–Te2	118.1(2)	Te1–Cu2–Te2	110.7(2)

sample for the purpose of temperature and voltage measurements. After achieving temperature equilibrium, the sample chamber was evacuated to less than 4×10^{-5} Torr. Small steady temperature gradients (maximum ~ 2 K) were obtained by incrementally increasing the power to the resistor. The resulting temperatures on both ends of the sample were measured. The voltages across the sample were also measured using the Chromel-*p* wires of the two thermocouples. A plot of sample voltages versus temperature gradients yielded a slope equal to the thermopower of the sample plus the thermopower of the Chromel-*p* wire. The absolute thermopower of the Chromel-*p* wire was subtracted from the measured slope to obtain the absolute thermopower of the sample (19). The overall accuracy of the thermopower measurement has been estimated from standards to be within $\pm$ 5%. Another plot of the power to the resistor divided by the area factor versus the temperature gradient gave a slope corresponding to the thermal conductivity of the sample. The overall accuracy of the thermal conductivity measurement has been estimated from standards of similar dimensions and thermal conductivity to be within $\pm$ 5% (19).

RESULTS AND DISCUSSION

Structural Analysis. $BaCu_2Te_2$ is isostructural to α-$BaCu_2S_2$ and $BaCu_2Se_2$ (17). The same structure type is adopted by $BaZn_2As_2$, $BaZn_2Sb_2$, and α-$ThNi_2P_2$ (20). In $BaCu_2Te_2$, the Cu and Te build up a three-dimensional framework and Ba atoms fill in the empty space (Fig. 2). The Ba atom is surrounded by seven Te atoms with bond distances from 3.4 to 3.6 Å. The coordination sphere can be described as a trigonal prism with one rectangular face capped by one Te atom. There are two crystallographically independent Cu sites. Both Cu atoms are coordinated to four Te atoms to form distorted $CuTe_4$ tetrahedra. Such a distortion of $CuTe_4$ tetrahedra is a feature frequently observed in Cu chalcogenides. In isostructural compounds, $BaZn_2As_2$, $BaZn_2Sb_2$, and α-$ThNi_2P_2$, distorted tetrahedra also appear, in the forms of $ZnAs_4$, $ZnSb_4$, and NiP_4, respectively. As shown in Fig. 2, the two distinct $CuTe_4$ tetrahedra (Cu1 and Cu2 tetrahedra) in $BaCu_2Te_2$ form one-dimensional columns along the *y* direction by edge-sharing. Between columns, $CuTe_4$ tetrahedra connect into a three-dimensional framework by corner-sharing. The shortest Cu–Cu distance is 2.847 Å and is a Cu2–Cu2 distance, suggesting at best weak Cu–Cu interactions.

In order to better understand the structure of the (Cu_2Te_2) sublattice, let us decompose the three-dimensional (Cu_2Te_2) framework and reassemble it back into a whole piece. A two-dimensional net is abstracted and projected in Fig. 3. The CuTe ladders run vertically across the page and they are connected at every second atom position, forming distorted hexagonal bridges between parallel ladders. These 2-D layers are then linked to a 3-D net, generated by

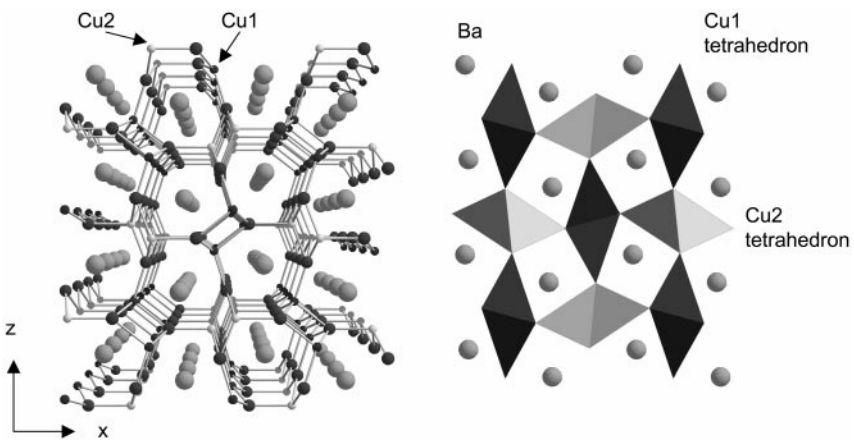

FIG. 2. The three-dimensional framework of $BaCu_2Te_2$ and the polyhedron presentation of $BaCu_2Te_2$.

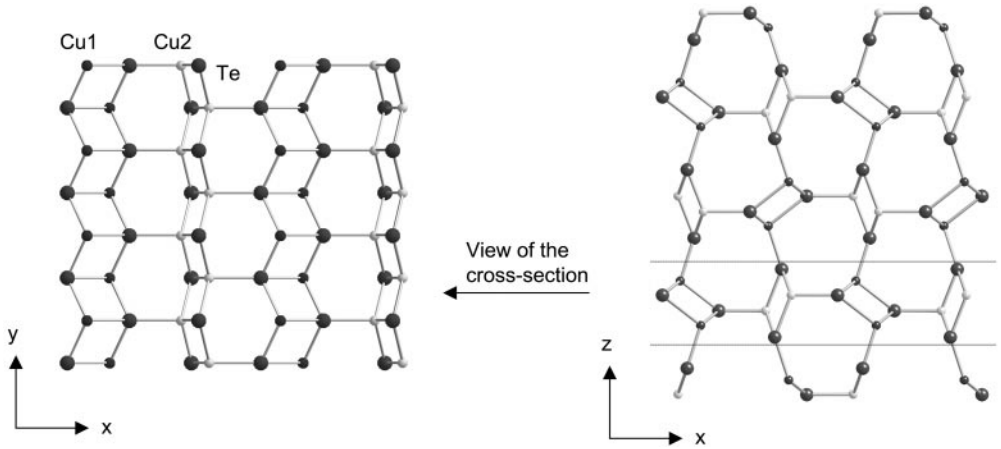

FIG. 3. Buildup of the 3-D (Cu_2Te_2) net from 2-D slabs.

a symmetry operation a (x, y, $\frac{1}{4}$), which is a glide reflection with the glide component ($\frac{1}{2}$, 0, 0) through the plane (x, y, $\frac{1}{4}$).

Now we make a connection between the $BaCu_2Te_2$ and the feldspar minerals with a general formula of $A(Al, Si)_4O_8$ (21–24), where A is alkali or alkaline earth metal. In the feldspar structure, the A cation is used to neutralize the negative charge of the $(Al, Si)_4O_8$ framework. Four vertices of each $(Al, Si)O_4$ tetrahedron are shared, which therefore leads to a net composition of $(Al, Si)O_2$ in the formula. Remarkably, if the $(Al, Si)O_4$ tetrahedra are viewed as the basic units and placed on the atomic positions shown in Fig. 3, the feldspar net is topologically the same as the (Cu_2Te_2) net. For comparison, the structure of the mineral Celsian ($BaAl_2Si_2O_8$, space group $I2/c$) (21–24) is shown in Fig. 4. The angles of the ladders and the relative orientation of the ladders are different between the feldspar net and the $BaCu_2Te_2$ net, but clearly Celsian is topologically identical to $BaCu_2Te_2$.

It is also interesting to compare the ternary $BaCu_2Te_2$ structure with the binary Nowotny phase of Cu_2Te (25). Cu_2Te crystallizes in $P6/mmm$. It is a layered compound composed of hexagonal Te and Cu layers stacked in the z direction, as shown in Fig. 5. The repeat sequence is Te–Te–Cu–Cu. The closest Te–Te distance is 2.828 Å and the closest Cu–Cu distance is 2.328 Å, both along the z direction. The covalent radii are 1.36 Å for Te and 1.17 Å for Cu (26), respectively. Obviously, there is strong covalent bonding in Te–Te and Cu–Cu along the z direction so that we could regard Te_2 and Cu_2 pairs as the basic geometric and electronic units in the compound. The Te_2 pairs build up a hexagonal 2-D slab with an interpair distance at 4.237 Å. The Cu_2 pairs are also arranged in a planar hexagonal pattern, but with an interpair distance at 2.446 Å,

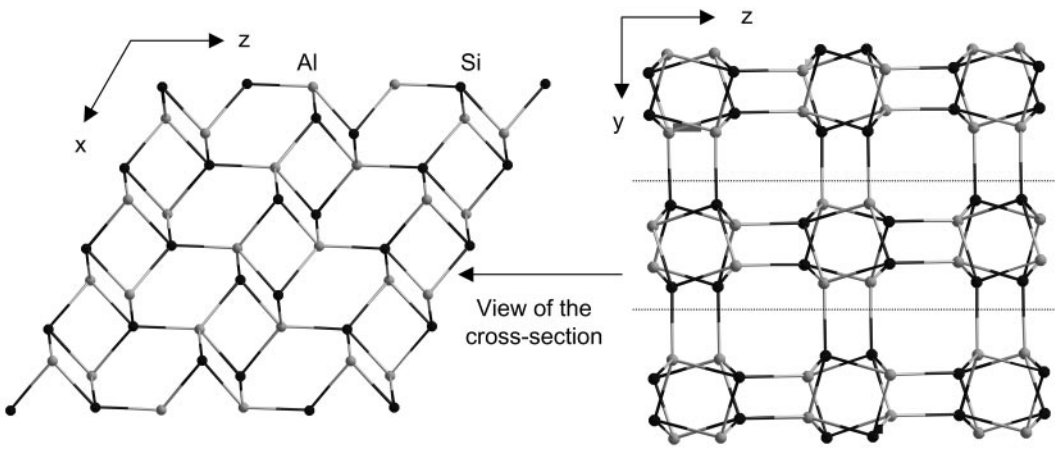

FIG. 4. From 2-D slab to the 3-D framework for Celsian $BaAl_2Si_2O_8$ (space group $I2/c$). Projections of the feldspar net on (010) and (100) are on the left and right, respectively. Only Al and Si are shown in the drawing to emphasize the net connection. O and Ba are omitted. In the real structure, Al and Si are tetrahedrally coordinated to four O atoms.

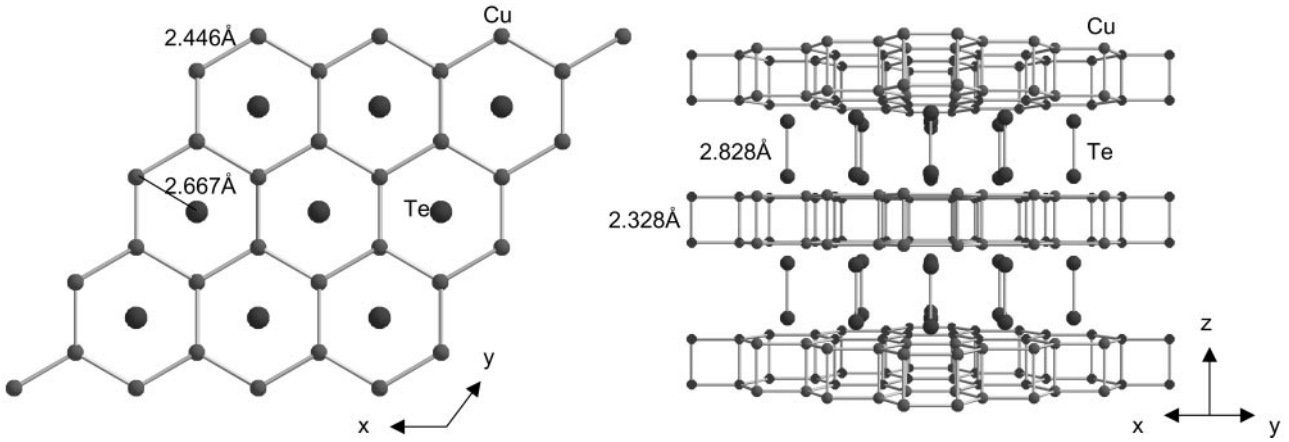

FIG. 5. The structure of Cu_2Te (*P6/mmm*).

compared with the Cu–Cu distance of 2.556 Å in Cu metal (27). The Cu_2 slabs are twice as dense as the Te_2 slabs. Now the repeat sequence of the crystal structure can be described as Te_2–Cu_2 along the z direction. Due to the formation of Te–Te pairs, the formal oxidation states in Cu_2Te can be described as Te^{1-} and $Cu^{0.5+}$. However, the formal oxidation state assignment for $BaCu_2Te_2$ is Ba^{2+}, Cu^{1+}, and Te^{2-}, following the Zintl–Klemm formalism (28). Obviously, there is no structural or electronic similarity between $BaCu_2Te_2$ and Cu_2Te.

Transport Properties. Figure 6 shows the four-probe electrical resistivity data measured on a sintered powder pellet of $BaCu_2Te_2$. The sample displays good electrical conductivity over the entire temperature range: 3.8 m$\Omega\cdot$cm at 30 K and 7.9 m$\Omega\cdot$cm at 295 K. The resistivity decreases as the temperature decreases and the decrease is not so significant as expected for a typical metal. This suggests that the compound is a degenerate semiconductor as prepared. A noticeable result in the ρ–T curve is the anomaly around 60–70 K. It was observed in both the cooling and heating runs. Similar anomalies in transport properties have been found in β-$Cu_{2-x}Se$ and $Cu_{2-x}Te$ and attributed to phase transitions (11, 13, 29). Cu_2Te undergoes four polymorphic transitions at 180, 305, and 460–555°C (11, 13). Cu_2Se has two polymorphs: a low-temperature phase α-Cu_2Se stable up to approx. 130°C and a high temperature phase β-Cu_2Se (29a, b). Phase transitions are not rare in copper chalcogenides (29, 30), and are usually associated with changes in Cu ion conductivity.

Table 4 summarizes the thermopower, thermal conductivity, and L/L_0 for the $BaCu_2Te_2$ sample at three temperatures. The magnitude of thermopower for $BaCu_2Te_2$ is in the range of doped semiconductors: 88 μV/K at room temperature and 29 μV/K at 89 K. The positive sign of S suggests that the dominant carriers are holes. The thermal conductivity κ increases from 22 mW/cm$\cdot$K at room temperature to 28 mW/cm$\cdot$K at 89 K. The thermal conductivity is composed of two parts; $\kappa = \kappa_{el} + \kappa_{ph}$, where κ_{el} is the contribution from electronic carriers (holes and electrons) and κ_{ph} is from phonon modes (lattice vibration). In typical metals, the electronic contribution dominates, which is generally one or two orders of magnitude larger than the phonon contribution. In this case, the Wiedemann–Franz law holds and the Lorentz number ($L = \rho\kappa/T$) is

$$L_0 = \frac{p^2}{3}\left(\frac{k_B}{e}\right)^2 = 2.44 \times 10^{-8}\,(\mathrm{V/K})^2. \qquad [1]$$

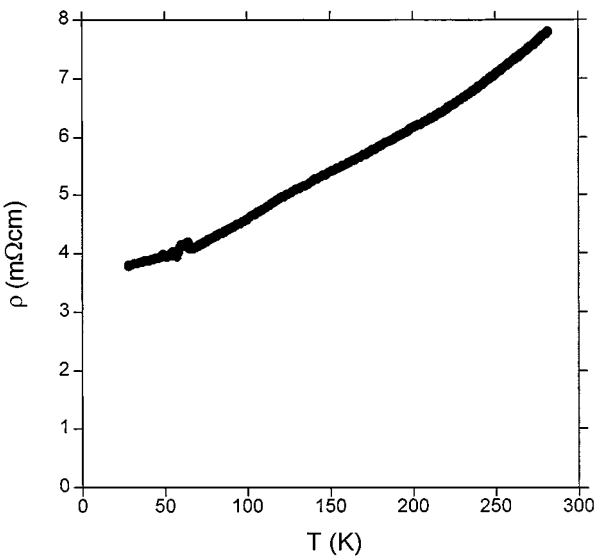

FIG. 6. The temperature dependence of electrical resistivity for the $BaCu_2Te_2$ sample.

TABLE 4
Thermopower, Thermal Conductivity, and L/L_0 for the $BaCu_2Te_2$ Pellet

T(K)	S (μV/K)	κ (W/cm·K)	ρ (mΩ·cm)	L/L_0
297	88.3	0.0225	7.959	24.7
139	42.8	0.0237	5.260	36.8
88.9	29.2	0.0276	4.424	56.3

In semiconductor and insulators, due to charge carrier densities much lower than those in metals, the contribution from phonons is usually significant and dominant. If $L/L_0 > 1$, it means that the phonon contribution to the total thermal conductivity is dominant. As shown in Table 4, the L/L_0 values for $BaCu_2Te_2$ are 25 at room temperature and 56 at 89 K. This clearly shows that the phonon contribution to the thermal conductivity is dominant. When the temperature decreases, the L/L_0 values increase dramatically. At lower temperatures, the phonon contribution becomes more important, presumably due to lower phonon–phonon scattering in this semiconducting compound.

Conclusion. In the spirit of the Zintl–Klemm concept (28), the formal oxidation state in $BaCu_2Te_2$ can be described as Ba^{2+}, Cu^{1+}, and Te^{2-}. The (Cu_2Te_2) framework has a charge of $2-$. The valence-precise characteristic predicts semiconducting behavior. An extended Hückel tight-binding band structure calculation performed on the sublattice $(Cu_2Te_2)^{2-}$ yielded a band gap of approximately 5 eV (31). Extended Hückel calculations are known to overestimate the band gap, but the computations unambiguously demonstrate that this compound is semiconducting. The transport property measurements on a sintered pellet of $BaCu_2Te_2$ suggest that it is a *p*-type degenerate semiconductor. Degenerate behaviors can result from impurities or defects that produce a carrier density in excess of about $10^{18}/cm^3$. A reversible anomaly was observed in the electrical resistivity near 65 K, possibly indicating a phase transition at the temperature. The phonon contribution to the thermal conductivity is dominant in the sample.

ACKNOWLEDGMENT

This work was funded by the Office of Naval Research.

REFERENCES

1. (a) R. A. Munson, W. DeSorbo, and J. S. Kouvel, *J. Chem. Phys.* **47,** 1769 (1967). (b) W. Meissner, *Z. Phys.* **58,** 570 (1929). (c) D. Shoenberg, *Nature* **142,** 874 (1938). (d) R. M. Fleming, L. W. ter Haar, and F. J. DiSalvo, *Phys. Rev. B* **35,** 5388 (1987).
2. (a) X. Zhang and M. G. Kanatzidis, T. Hogan, and C. R. Kannewurf, *J. Am. Chem. Soc.* **118,** 693 (1996). (b) X. Zhang, T. Hogan, C. R. Kannewurf, and M. G. Kanatzidis, *J. Alloys Compd.* **236,** 1 (1996). (c) X. Zhang, Y. Park, T. Hogan, J. L. Schindler, C. R. Kannewurf, S. Seong, T. Albright, and M. G. Kanatzidis, *J. Am. Chem. Soc.* **117,** 10,300 (1995). (d) X. Zhang, J. L. Schindler, T. Hogan, J. Albritton-Thomas, C. R. Kannewurf, and M. G. Kanatzidis, *Angew. Chem. Int. Ed. Engl.* **34,** 68 (1995). (e) Y. Park and M. G. Kanatzidis, *Chem. Mater.* **3,** 781 (1991).
3. (a) F. Q. Huang, P. Brazis, C. R. Kannewurf, and J. A. Ibers, *J. Am. Chem. Soc.* **122,** 80 (2000). (b) F. Q. Huang and J. A. Ibers, *Inorg. Chem.* **38,** 5978 (1999). (c) P. M. Keane, Y. -J. Lu, and J. A. Ibers, *Acc. Chem. Res.* **24,** 223 (1991). (d) P. M. Keane and J. A. Ibers, *Inorg. Chem.* **30,** 3096 (1990).
4. G. Vajenine and R. Hoffmann, *Inorg. Chem.* **35,** 451 (1996).
5. (a) C. S. Sunandana, Y. L. Saraswathi, and P. S. Kumar, *Indian J. Pure Appl. Phys.* **37,** 325 (1999). (b) G. Dagan, T. F. Ciszek, and D. Cahen, *J. Phys. Chem.* **96,** 11,009 (1992). (c) R. C. T. Slade and N. Singh, *Solid State Ionics* **58,** 9 (1992). (d) M. Horvatic and Z. Vucic, *Solid State Ionics* **13,** 117 (1984).
6. (a) J. W. Gardner, *Engl. Electr. J.* **18,** 16 (1963). (b) W. Lehmunn, *J. Electrochem. Soc.* **104,** 45 (1957). (c) D. A. Cusano, *Solid State Electron.* **6,** 217 (1963). (d) M. Aven and D. A. Cusano, *J. Appl. Phys.* **35,** 606 (1964). (e) P. J. Mosticat, *Phys. Stat. Solid.* **11,** 531 (1972).
7. B. Li, Y. Xie, J. X. Huang, H. L. Su, and Y. T. Qian, *J. Solid State Chem.* **146,** 47 (1999).
8. B. S. Farag and S. A. Khodier, *Thin Solid Films* **201,** 231 (1991); *Thin Solid Films* **205,** 52 (1991).
9. O. P. Astakhov, *Neorg. Mater.* **11,** 23 (1975).
10. G. P. Sorokin, G. Z. Idrichan, and Z. M. Sorokina, *Neorg. Mater.* **11,** 1357 (1975).
11. R. Blachnik, M. Lasocka, and U. Walbrecht, *J. Solid State Chem.* **48,** 431 (1983).
12. J. W. Gardner, *World Power Eng.* **1,** 22 (1963).
13. B. Mansour, F. Mukhtar, and G. G. Barakati, *Phys. Stat. Sol.* (*a*) **95,** 703 (1986).
14. K. Sridhar and K. Chattopadhyay, *J. Alloy. Compd.* **264,** 293 (1998).
15. K. O. Klepp, *J. Less-Common Met.* **128,** 79 (1987).
16. M. Onoda and M. Saeki, *Mater. Res. Bull.* **24,** 1337 (1989).
17. J. E. Iglesias, K. E. Pachali, and H. Steinfink, *J. Solid State Chem.* **9,** 6 (1974).
18. A. C. Larson and R. B. Von Dreele, "General Structure Analysis System." Los Alamos National Laboratory.
19. C. D. W. Jones, K. A. Regan, and F. J. DiSalvo, *Phys. Rev. B* **58,** 16,057 (1998).
20. (a) E. Brechtel, G. Cordier, and H. Schaefer, *Z. Naturforsch. B* **34,** 921(1979). (b) P. Kluefers and A. Mewis, *Z. Naturforsch. B* **33,** 151 (1978). (c) J. H. Albering and W. Jeitschko, *Z. Naturforsch. B* **49,** 1074 (1993).
21. M. O'Keeffe and B. G. Hyde, "Crystal Structures—I. Patterns and Symmetry," pp. 313–315. Mineralogical Society of America, Washington, 1996.
22. N. N. Greenwood and A. Earnshaw, "Chemistry of the Elements," pp. 414–416. Pergamon Press, Oxford, 1984.
23. A. F. Wells, "Structural Inorganic Chemistry," pp. 1033–1042. Clarendon Press, Oxford, 1984.
24. D. Palmer, CrystalMaker 4.0, Minerals Libraries.
25. (a) H. Nowotny, *Z. Matallk.* **37,** 40 (1946). (b) I. Patzak, *Z. Matallk.* **47,** 418 (1956).
26. "Table of Periodic Properties of the Elements," Sargent-Welch Scientific Company, 1994.
27. L. Pauling, "The Nature of the Chemical Bond," p. 410. Cornell University, Ithaca, NY.

28. (a) E. Zintl and W. Dullenkopf, *Z. Phys. Chem. B* **16,** 183 (1932). (b) E. Zintl and G. Brauer, *Z. Phys. Chem. B* **20,** 245 (1933). (c) E. Zintl, *Angew. Chem.* **52,** 1 (1939). (d) W. Klemm, *Z. Anorg. Allg. Chem.* **247,** 1 (1941).
29. (a) R. D. Heyding, *Can. J. Chem.* **44,** 1233 (1966). (b) M. A. Korzhuev, *Phys. Solid State* **35,** 1497 (1993). (c) V. M. Glazov and A. S. Burhanov, *Neorg. Mater.* **19,** 1986 (1983). K. Dovletov, S. N. Krzivitskaya, N. K. Samakhotina, K. Tashliev, and Kh. Erniyazov, *Neorg. Mater.* **18,** 754 (1982).
30. J. E. Iglesias, K. E. Pachali, and H. Steinfink, *Mat. Res. Bull.* **7,** 1247 (1972).
31. (a) R. Hoffmann, *J. Chem. Phys.* **39,** 1397 (1963). (b) G. Landrum, "Yet Another Extended Hückel Molecular Orbital Package (YAeHMOP)," Cornell University, 1997. YAeHMOP is available on the World Wide Web at http://overlap.chem.cornell.edu:8080/yaehmop.html. (c) The following valence shell ionization potentials (H_{ii} in eV), orbital exponents (ζ), and the weighting coefficients c were used in the calculation: Cu $4s\zeta = 2.2$, $H_{ii} = -11.4$; Cu $4p\zeta = 2.2$, $H_{ii} = -6.06$; Cu $3d\zeta_1 = 5.95$ and $c_1 = 0.5933$, $\zeta_2 = 2.30$ and $c_1 = 0.5744$, $H_{ii} = -14.0$; Te $5s\zeta = 2.51$, $H_{ii} = -20.8$; Te $5p\zeta = 2.16$, $H_{ii} = -14.8$.